

A Model For Energy Transfer in Collisions of Atoms with Highly Excited Molecules

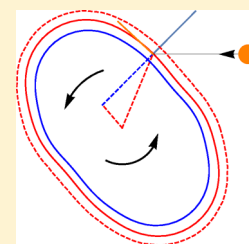
Paul L. Houston,^{*,†} Riccardo Conte,^{*,‡} and Joel M. Bowman^{*,‡}

[†]School of Chemistry and Biochemistry, Georgia Institute of Technology, Atlanta, Georgia 30332, United States

Department of Chemistry and Chemical Biology, Cornell University, Baker Laboratory, Ithaca, New York 14852, United States

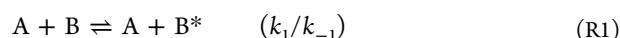
[‡]Department of Chemistry and Cherry L. Emerson Center for Scientific Computation, Emory University, Atlanta, Georgia 30322, United States

ABSTRACT: A model for energy transfer in the collision between an atom and a highly excited target molecule has been developed on the basis of classical mechanics and turning point analysis. The predictions of the model have been tested against the results of trajectory calculations for collisions of five different target molecules with argon or helium under a variety of temperatures, collision energies, and initial rotational levels. The model predicts selected moments of the joint probability distribution, $P(J_{\beta}, \Delta E)$ with an $R^2 \approx 0.90$. The calculation is efficient, in most cases taking less than one CPU-hour. The model provides several insights into the energy transfer process. The joint probability distribution is strongly dependent on rotational energy transfer and conservation laws and less dependent on vibrational energy transfer. There are two mechanisms for rotational excitation, one due to motion normal to the intermolecular potential and one due to motion tangential to it and perpendicular to the line of centers. Energy transfer is found to depend strongly on the intermolecular potential and only weakly on the intramolecular potential. Highly efficient collisions are a natural consequence of the energy transfer and arise due to collisions at “sweet spots” in the space of impact parameter and molecular orientation.



INTRODUCTION

The Lindemann mechanism is essential to the understanding of many chemical reactions. These include reactions in combustion chemistry, atmospheric chemistry, explosions, and interstellar chemistry, to name a few. Although it is now nearly a century old,^{1,2} many details of this mechanism are still poorly understood. It has two seemingly simple steps:



where A is typically an atom or small molecule, B is the target molecule, and B* is the target molecule with vibrational and/or rotational excitation.

We have previously summarized some of the important work on this mechanism,^{3,4} and the field has been extensively reviewed elsewhere.^{5–11} Thus, only a brief overview will be provided here. Experimental techniques have generated a wealth of data on this process. Some of the more important methods are chemical activation,¹² time-resolved spontaneous infrared fluorescence,^{13–15} time-resolved ultraviolet absorption,^{16–18} kinetically controlled selective ionization (KCSI),¹⁹ high-resolution transient IR absorption spectroscopy,^{20,21} mass spectroscopy,²² and time-sliced ion imaging.²³ Theoretical and computational studies have also been informative.^{3,10,24–33} Of particular interest to the current study are the computational investigations of argon collisions with ethane and pyrazine,¹⁰ with methane,^{30,31} with HOCO,³³ with the allyl radical,^{3,32} and of helium with methane.²⁹

The goal of the current work is to develop a model for energy transfer in atomic collisions with highly excited molecules. The reasons for wanting such a model are two-fold. First, a successful model shows what properties and concepts are most important to the energy transfer process. Second, by delineating what is most important in a particular process, a successful model often suggests computational approximations that can be used to make calculating the desired results more efficient.

Several models have previously been reported. Early work by Barker applied SSH theory to the energy transfer process.³⁴ More recent work includes the approach by Nordholm and colleagues,^{35–42} who apply ergodic collision theory to the energy transfer problem. Their model, when adjusted to reflect the fact that not all collisions are strong, gives good agreement with a variety of experiments.⁴³ We have previously reported a very simple model that with a few adjustable parameters fits the results of many computational studies.⁴ However, a disadvantage of this model is that it does not provide a method for estimating the values of the adjustable parameters. The model presented here has no adjustable parameters; the input parameters are properties of the atom and molecule and of their intermolecular potential. The model explicitly takes into account the shape and mass distribution of the target molecule. The result of a simple calculation (about one CPU-hour) is the joint probability distribution (JPD), $P(J_{\beta}, \Delta E)$, which gives the

Received: January 8, 2015

Revised: April 23, 2015

Published: April 24, 2015

probability that a transition will be made from J_i to J_f and from E_i to $E_i + \Delta E$, where it is assumed that J_i and E_i either are known or can be calculated from thermal distributions.

The JPD can be used to calculate any desired moment, $\langle \Delta E^m \Delta J^m \rangle$, characterizing the energy transfer process. Jasper and colleagues⁴⁴ have recently shown that, given such moments, it is possible to accurately calculate the pressure-dependent kinetics of a chemical reaction. In their method, the moments are calculated by performing trajectory calculations. The model proposed here allows much more rapid calculation of the joint probability distribution and its moments. It should thus make possible more efficient calculations of pressure-dependent reaction rates.

The model presented here is successful in predicting the JPD following a single collision from initial conditions selected by microcanonical sampling. It is based primarily on classical mechanics and obeys detailed balance. It does not address what happens after multiple collisions, so it does not rely on or predict the thermodynamic outcome of such multiple collisions. The model is intended to provide input data for a master equation model, as well as to provide a better understanding of energy transfer in highly excited molecules.

Several physical insights are available from the model. First, rotational energy transfer in highly excited molecules is more probable than vibrational energy transfer; the latter can be considered a perturbation on the former. Second, an accurate calculation of the results of rotational energy transfer can be obtained using only the intermolecular potential in conjunction with conservation laws. Third, rotation changing collisions are induced by two mechanisms, one involving motion in the direction normal to the potential energy contours, and a second involving motion tangent to the contours and perpendicular to the line-of-centers (LOC). Fourth, highly efficient collisions (HECs) occur naturally for high- J_i systems as a result of collisional “sweet spots” where substantial rotational and vibrational energy can be exchanged.

Table 1 provides a list of acronyms used in the manuscript.

Table 1. List of Acronyms Used in the Manuscript

acronym	meaning
COM	center of mass
GM	global minimum
HEC	highly efficient collision
JPD	joint probability distribution
lhs	left-hand side
LOC	line of centers
rhs	right-hand side
TP	turning point

MODEL

Outline of the Model. The model is developed in two stages. First, we analyze motion for a rigid molecule in its equilibrium configuration interacting with an atom through a three-dimensional intermolecular potential $V(\mathbf{R})$, where $\mathbf{R} = \{x, y, z\}$ is the position of the atom relative to the center of mass (COM) of the molecule at $\mathbf{R} = \{0, 0, 0\}$. Turning points (TPs) are then determined for random orientations of the molecule with respect to the incoming atom and for initial impact parameters taken between $b_i = 0$ and $b_i = b_{\max}$ from a probability distribution $dP(b) = 2\pi b db$. The turning points are

calculated using a straight-line approximation and the intermolecular potential.

An arbitrary unit vector is chosen for the direction of the initial rotational angular momentum, \mathbf{J}_i , of magnitude J_i . When there is rotational energy transfer only, then for each turning point the conservation equations for angular momentum and energy can be solved to find J_f , the final rotational state of the molecule, as well to determine its direction relative to the axes of the molecule. This direction determines the moment of inertia that is relevant for calculating the associated rotational energy change, which is also ΔE for the collision under the assumption that only rotational energy transfer occurs. The joint probability distribution $P(J_f, \Delta E)$ is just given by the number of turning points that give these values of J_f and ΔE divided by the total number of turning points considered.

In the second stage, we allow the possibility that vibrational energy can be transferred, and this energy must be taken into account when considering the conservation laws. The model assumes that the probability for the vibrational energy exchange is given by the adiabaticity principle, but that there are also limitations on the amount of vibrational energy that can be transferred depending on the turning point. We calculate the amount of vibrational energy transferred by using Morse potentials to evaluate the degree to which the molecule vibrates. The value of ΔE is then augmented or diminished by the energy change at the turning point due to the vibration of the target molecule. In the case when only $V \leftrightarrow T$ transfer is allowed, all of the vibrational energy is used to change ΔE , whereas if $V \leftrightarrow R$ transfer is also allowed, not all of the vibrational energy changes ΔE because that fraction of it that is transferred to rotation does not change the internal energy of the molecule.

In summary, the first level of approximation treats the rotational exchange exactly to within the straight-line trajectory assumption and captures much of the physics of the energy transfer. With a second or third level of approximation, there is a broadening of the ΔE values or both the ΔE and J_f values due to the vibration of the molecule. This broadening increases the agreement of the model with the results of trajectory calculations. In particular, it allows successful modeling of the downward energy transfer for systems with $J_i = 0$. However, we find that the vibrational energy change is basically a perturbation on the solution to rotational exchange.

Details of the Model. We calculate the turning point with a straight-line trajectory approximation using the intermolecular potential, a selected impact parameter, and a fixed but randomly chosen molecular orientation. For trajectories that reach the repulsive region of the potential, the turning point is defined as the point at which the potential is equal to the collision energy, as evaluated from the velocity component in the direction normal to the potential. For straight-line trajectories that do not reach the repulsive region, we define the turning point as the point on the incoming trajectory for which the distance along the gradient to the point where $V(\mathbf{R}) = 0$ is a minimum. This conforms most closely to the definition used in the trajectories as the distance of closest approach, although the agreement is only approximate.

Conservation of angular momentum is summarized by the vector equation

$$\mathbf{L}_i + \mathbf{J}_i = \mathbf{L}_f + \mathbf{J}_f \quad (1)$$

where the vectors are the initial and final orbital and rotational angular momenta of the system.

Conservation of energy is summarized by the scalar equation

$$E_{i,\text{trans}} + E_{i,\text{internal}} = E_{f,\text{trans}} + E_{f,\text{internal}} \quad (2)$$

or

$$\Delta E = E_{f,\text{internal}} - E_{i,\text{internal}} = E_{i,\text{trans}} - E_{f,\text{trans}} = -\Delta E_{\text{trans}} \quad (3)$$

where ΔE is the change in the target molecule's internal energy, which must be equal to the negative of the change in the translational energy of the atom–molecule pair. Because $L_i = \mu v_i b_i$ and $L_f = \mu v_f b_f$, eqs 1 and 2 can be combined by using the initial and final impact parameters:

$$\Delta E = (1/2)\mu \left(\frac{L_i}{\mu b_i} \right)^2 - (1/2)\mu \left(\frac{L_f}{\mu b_f} \right)^2 \quad (4)$$

where the values in the parentheses are the initial and final relative velocities and b_i and b_f are the initial and final impact parameters, respectively. The first term on the rhs of 4 is simply equal to the initial relative energy E_{rel} . Thus,

$$\Delta E = E_{\text{rel}} - (1/2)\mu \left(\frac{L_f}{\mu b_f} \right)^2 \quad (5)$$

From 1 we see that L_f is the magnitude of $\mathbf{L}_i - \Delta \mathbf{J}$, where $\Delta \mathbf{J} = \mathbf{J}_f - \mathbf{J}_i$. Consequently,

$$\Delta E = E_{\text{rel}} - (1/2)\mu \left(\frac{|\mathbf{L}_i - \Delta \mathbf{J}|}{\mu b_f} \right)^2 \quad (6)$$

Although eq 6 gives the solution to the conservation laws that relates ΔE to $\Delta \mathbf{J} = \mathbf{J}_f - \mathbf{J}_i$, it is difficult to use. Typically, although L_i is known from the initial conditions, ΔE depends on $\Delta \mathbf{J}$ through both the dependence of rotational energy on $\Delta \mathbf{J}$ and the dependence of the rotational constant on the direction of $\Delta \mathbf{J}$. Additionally, we do not typically know b_f . However, these problems may be overcome in the straight-line trajectory approximation by separating the incoming and outgoing velocities into judiciously chosen components. Let \mathbf{v}_{rel} be the initial velocity corresponding to E_{rel} . By separating this initial velocity into components normal and tangential to the equipotential contour of $V(\mathbf{R})$ at the turning point, we have $\mathbf{v}_{\text{rel}} = \mathbf{v}_{i,n} + \mathbf{v}_{i,t}$. Let the energies corresponding to these velocities be E_n and E_t . Furthermore, we decompose $\mathbf{v}_{i,t}$ into components perpendicular and parallel to the line of centers (LOC), defined as the line between the COM and the turning point. Then, $\mathbf{v}_{i,t} = \mathbf{v}_{i,t,\text{perp}} + \mathbf{v}_{i,t,\text{par}}$.

Now consider the motion along each of these three directions. For incoming motion along the normal, the equipotential contours perpendicular to the motion guarantee that the outgoing motion is also along the normal, so that the directions of $\mathbf{L}_{i,n}$ and $\mathbf{L}_{f,n}$ are along the same line but opposite to one another; thus, $\Delta \mathbf{J}_n$ must also be along this line. Similarly, motion in the tangential direction perpendicular to the LOC encounters a “hill” or “valley” in the potential. The incoming motion is along an equipotential contour and, to first order, the change in potential is perpendicular to this direction. Thus, the motion remains along the tangential direction as it encounters the potential, where it is reflected back on itself. Again, the directions of $\mathbf{L}_{i,t,\text{perp}}$ and $\mathbf{L}_{f,t,\text{perp}}$ are along the same line but opposite to one another; thus, $\Delta \mathbf{J}_{t,\text{perp}}$ must also be along the same line. Motion along the third direction tangential to the

normal and parallel to the LOC is unimportant for changes in rotation because the impact parameter is zero.

As we have just seen, for motion along the normal direction and along the tangential direction parallel to the LOC, the initial and final trajectories are along the same line, and thus the initial and final impact parameters are equal. As explained above, the vectors \mathbf{L}_i , $\Delta \mathbf{J}$, and \mathbf{L}_f are collinear, so that their vector addition can be replaced by the normal addition of their magnitudes. For example, along the normal direction, the initial and final impact parameters are equal to the shortest distance between the COM and a line that passes through the turning point and is parallel to the normal (or gradient) to the potential. Let this impact parameter be denoted by b_n . Then $L_{i,n} = \mu v_{i,n} b_n$ and $L_{i,n} - \Delta J_n = L_{i,n} - \Delta J_n$, so that

$$\Delta E(J_{i,n}, J_{f,n}) = E_n - (1/2)\mu \left(\frac{L_{i,n} - \Delta J_n}{\mu b_n} \right)^2 \quad (7)$$

where the dependence of ΔE on J_i and J_f has been made explicit, because by assumption so far, we are considering changes only in internal rotational energy. Because $\Delta J_n = J_{f,n} - J_{i,n}$, the equation can easily be solved for $J_{f,n}$ given $J_{i,n}$. The value of $J_{i,n}$ can be determined by the following procedure. The magnitude of the total initial rotational angular momentum, J_i , is given by the problem or selected from a rotational temperature. Given J_i , we choose an arbitrary axis for the initial rotation and project \mathbf{J}_i onto the direction of $\Delta \mathbf{J}_n$ to find $J_{i,n}$. We will then need to average over initial rotational axes as well as over the TPs. The direction for $\Delta \mathbf{J}_n$ is determined from the turning point analysis (see below for the calculation of this direction).

Similar equations hold for motion along $\mathbf{v}_{t,\text{perp}}$, where E_n is replaced by $E_{t,\text{perp}}^{\text{min}}$ and $b_{t,\text{perp}}$ is equal to the distance from the COM to the turning point, and for motion along $\mathbf{v}_{t,\text{par}}$, where E_n is replaced by $E_{t,\text{par}}$ and $b_{t,\text{par}} = 0$. In the former case, the combined conservation equation is thus

$$\Delta E(J_{i,t}, J_{f,t}) = E_{t,\text{perp}}^{\text{min}} - 1/2\mu \left(\frac{L_{i,n} - \Delta J_n}{\mu b_{t,\text{perp}}} \right)^2 \quad (8)$$

In the latter case, as mentioned earlier, the velocity does not contribute to the angular momentum (i.e., there is an elastic exchange of momenta) and $\Delta J_{t,\text{par}}$ is zero. As shown in Figure 2 of ref 4, $E_{t,\text{perp}}^{\text{min}}$ is given by the smaller of the value of the potential at the turning point and the value of $E_{t,\text{perp}} = (1/2)\mu v_{t,\text{perp}}^2$.

For motions along \mathbf{v}_n and along $\mathbf{v}_{t,\text{perp}}$, eqs 7 and 8 can easily be solved for $J_{f,n}$ and $J_{f,t}$ respectively. There are, in principle, as many as two solutions to each equation, but in many cases the only physically realistic solution is the trivial one for which $J_f = J_i$, i.e., for which the collision is elastic.

The directions of all vectors in the equation $\mathbf{J}_f = \mathbf{J}_{f,n} + \mathbf{J}_{f,t}$ are needed to determine the rotational constants, which, for this classical approach, are simply related to the moments of inertia around corresponding rotational vectors. For motion along \mathbf{v}_n , the direction of $\Delta \mathbf{J}_n$ is given by $\mathbf{v}_n \times \mathbf{b}_n$, where \mathbf{b}_n is a vector of length b_n from the COM to the nearest point on a line through the turning point and parallel to the normal to the potential surface. For motion along $\mathbf{v}_{t,\text{perp}}$, the direction of $\Delta \mathbf{J}_{t,\text{perp}}$ is given by $\mathbf{v}_{t,\text{perp}} \times \mathbf{b}_{t,\text{perp}}$, where $\mathbf{b}_{t,\text{perp}}$ is a vector of length $b_{t,\text{perp}}$ from the COM to the turning point. For many initial \mathbf{J}_i directions, the projection onto $\Delta \mathbf{J}_n$ or $\Delta \mathbf{J}_{t,\text{perp}}$ will be negative. Positive projections correspond to cases where \mathbf{L}_i is in the same

direction as the rotation, so that the collision increases J_y , whereas negative projections correspond to cases where L_i is in the opposite direction as the rotation, so that the collision decreases J_y . Once J_f is determined, the rotational constant may be calculated by determining the moment of inertia of the molecule about its direction and by then converting this moment into a rotational constant. We calculate J_f from $\mathbf{J}_f = \mathbf{J}_i - (\mathbf{J}_{i,n} + \mathbf{J}_{i,t}) + (\mathbf{J}_{f,n} + \mathbf{J}_{f,t})$. This step completes the solution of eq 6, from which we find for each turning point 1–4 pairs of values J_f and ΔE that are consistent with conservation of both energy and angular momentum for the situation when only rotational energy change is considered.

An example is helpful in understanding the arguments above. We consider solution of eqs 7 and 8 for motion normal to the potential surface and tangential to both the normal and the LOC, respectively. The specific case is for the allyl radical in its global minimum configuration. Euler angles of $\{\chi, \theta, \phi\} = \{0, 0, 0\}$ correspond to having all the atoms in the x - y plane with the major C–C–C axis along the x direction. For this particular example, the molecule is rotated but is still in the x - y plane. Figure 1 shows a depiction of the potential energy surface and of various vectors important in the analysis, as explained in the caption.

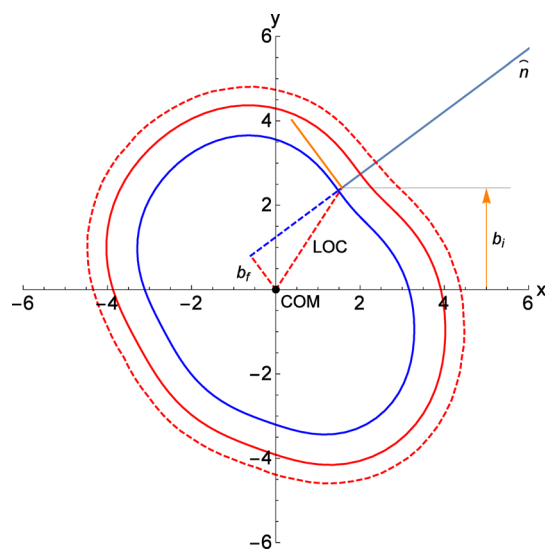


Figure 1. The blue contour is where $V(\mathbf{R}) = E_n$, the red contour is where $V(\mathbf{R}) = 0$, and the dashed red contour is where $V(\mathbf{R})$ is a minimum. The black line is the direction of the incoming atom with an impact parameter given by its y coordinate. The blue line is normal to the potential at the turning point, which is at the end of this line that is closest to the COM. The dashed blue line is the extension of the normal line to the point along this line closest to the COM. The dashed red line from this point to the COM has the length b_n . The dashed red line from the COM to the turning point is the line-of-centers. The solid orange line is the tangent to the surface at the turning point and is in the plane of the incident atom and the surface normal. The contours are for a cross section through the potential in the x - y plane, whereas the vectors are projected onto that plane.

Figure 2 depicts graphical solutions to eqs 7 and 8. The labeling is for the case of eq 7. There are in each case two conditions for solution, one for $J_{i,n} < 0$ shown in Figure 2a and one for $J_{i,n} > 0$ shown in Figure 2b. In each case, the rhs of the equation is represented by a parabola opening downward in ΔE . The dotted parts of the blue parabolae represent locations where L_f is positive and greater than L_y , a situation that is

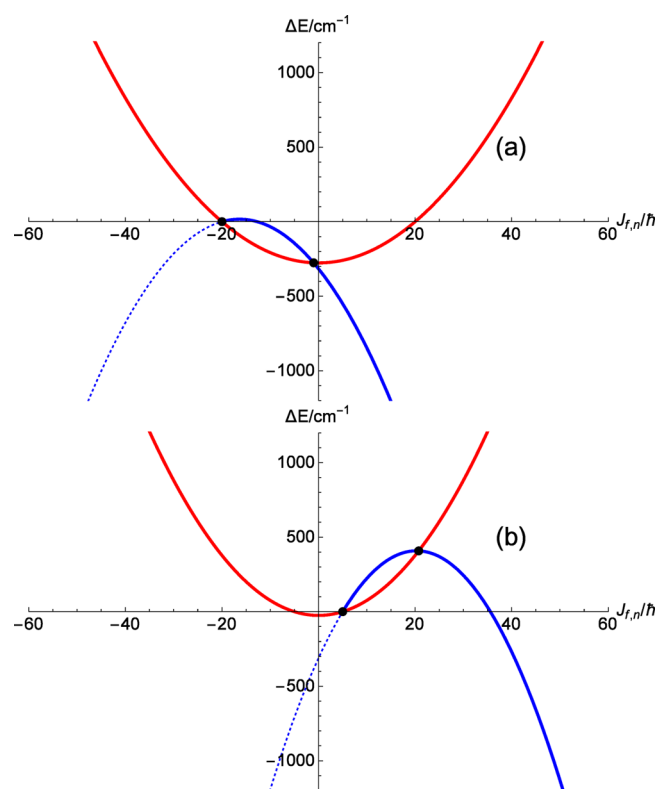


Figure 2. Graphical solution to eq 7 (intersections of solid lines). The red curves give the rotational energy, and the blue curves give $-\Delta E_{\text{trans}}$. The black dots give locations for $\{J_f, \Delta E\}$ that satisfy conservation of both energy and angular momentum. For this example, $J_{i,n} = -20$ in (a) and $J_{i,n} = 5$ in (b).

inconsistent with the model. The lhs of the equation is simply the difference in rotational energy, $(J_{f,n}^2 - J_{i,n}^2) B_{\text{rot}}$, which is also parabolic in shape but opening upward in ΔE . The red curve crosses the $\Delta E = 0$ axis at the elastic point, where $J_{f,n} = J_{i,n}$. The black dots in the figure depict the points $\{J_{f,n}, \Delta E\}$ that satisfy the conservation laws. For the case depicted in Figure 2a, $J_i = 30$, $J_{i,n} = -20$, and $J_{f,n} = -20$ or -1 , and for the case depicted in Figure 2b, $J_i = 30$, $J_{i,n} = 5$, and $J_{f,n} = 5$ or 20.7 . Given that the red parabolae must go through the elastic points, it is clear from the geometry that $J_{f,n} < 0$ when $J_{i,n} < 0$ (Figure 2a), and that $J_{f,n} > 0$ when $J_{i,n} > 0$ (Figure 2b). Note that when the magnitude $J_{i,n}$ is relatively large and negative, it is possible for the collision to cause loss of nearly all the rotational energy, as shown in the not atypical situation of Figure 2a.

The model to this point is based on angular momentum and energy conservation for an atom colliding with a rigid rotor under a realistic potential. Although it can reproduce the trajectory results fairly accurately, as we will see later, it cannot account for one important feature. When J_i is small, there is no probability for energy transfer more negative than the rotational energy corresponding to J_i . Specifically, when J_i is zero, there is no probability for any negative value of ΔE if the molecule is rigid. Trajectories using realistic potentials and allowing the target molecule to change its shape do show probability for negative values of ΔE , even for $J_i = 0$, and it seems intuitive that the reason is that the target molecule is not rigid—it vibrates. One way to look at this is that the energy at the turning point for the equilibrium configuration of the rigid molecule changes as the molecule vibrates. We model the amount of vibrational energy available for the collision as the difference in energy

between the turning point energy of the rigid molecule versus the turning point energy of the molecule in a new configuration allowed by vibration. The vibrational energy can then be used by the collision either for conversion to/from rotational energy, allowing some different final rotation levels than those calculated for the rigid molecule, or for conversion to/from translational energy. Implementation of this vibrational energy model requires knowledge of how the molecule vibrates.

There are many models that can be used to predict the atomic positions as the target molecule vibrates. An accurate one is to run a trajectory on the excited molecule with an appropriate intramolecular potential. Though accurate, this level of effort is probably more than needed, because the vibrational correction to the rotational solution is small. One method that seems partially successful is to make a simple force field model based on stretches only and to use that model to calculate atomic positions. Some of the comparisons reported below use trajectories to generate atomic positions, whereas some use this simple force field model. In the simple force field model, the stretching motion between each pair of bonded atoms is treated as a Morse oscillator using the masses of the atoms, generic tables for frequencies, and generic tables of bond dissociation energies. The amount of energy in each oscillator is given by equipartition, and the positions of the atoms are chosen by letting each bond take a distance sampled from the probability of observing that distance in the Morse oscillator.

We now suppose that vibrational energy is allowed to be exchanged from the target molecule either to/from the translational motion between the atom and molecule ($V \leftrightarrow T$ transfer) or to/from the rotational motion of the molecule ($V \leftrightarrow R$ transfer). Combinations of $\{\Delta E, J_f\}$ in addition to those calculated from eqs 7 and 8 would then be allowed. Let the change in internal energy ΔE be written as the sum of the changes in internal rotational energy and vibrational energy: $\Delta E = \Delta E_{\text{rot}} + \Delta E_{\text{vib}}$. The amount of energy that is taken from or added to vibration then adds to or subtracts from the final rotational and translational energies; that is, $\Delta E_{\text{vib}} = -[V_{\text{TP}}(\text{equilibrium}) - V_{\text{TP}}(\text{vibrated})]$, where “equilibrium” stands for the original configuration of the molecule and “vibrated” stands for the configuration of the molecule in its vibrationally stretched or compressed configuration.

If only $V \leftrightarrow T$ energy transfer occurs, then ΔJ is unchanged, while ΔE is changed by the value of ΔE_{vib} . If $V \leftrightarrow R$ exchange also occurs, then the result is somewhat more complicated. To the extent that ΔE_{rot} increases/decreases as ΔE_{vib} decreases/increases, ΔE is unchanged. But the only way to change ΔE_{rot} while conserving energy is to also change the translational energy. Thus, $V \leftrightarrow R$ exchange always also involves some $V \leftrightarrow T$ exchange. The model results described below can be presented in three ways. In the first, we assume no vibrational energy is transferred, in the second, we assume that only $V \leftrightarrow T$ energy transfer occurs, whereas in the third we assume that $V \leftrightarrow R$ transfer also occurs. The $V \leftrightarrow T$ transfer has the effect of broadening the JPD in the ΔE dimension, whereas the $V \leftrightarrow R$ transfer has the effect of broadening the JPD in the ΔJ (or J_f) dimension. The $V \leftrightarrow R$ transfer also has the effect of increasing probability slightly for large ΔJ transitions.

The remaining question is how to calculate the probability for the situation in which both rotational and vibrational energy contribute to the change in internal energy. We assume that this probability is the product of a probability for the rotational energy change times a probability for the vibrational energy

change. Because we are averaging over the initial rotational axes, the probability for rotational transfer may be taken to be

$$P_{\text{rot}} = 1 \quad (9)$$

that is, every solution to the eqs 7 and 8 is given the same probability.

The vibrational probability, as in our previous paper,⁴ is assumed to be controlled by the adiabaticity principle. The probability is given by a density of states ratio times $\exp(-\tau_c/\tau_v)$, where τ_c is the collision time and τ_v is the vibrational period:

$$P_{\text{vib}} = \frac{\rho(E_i + \Delta E_{\text{vib}})}{\rho(E_i)} \exp[-\tau_c/\tau_v] \quad (10)$$

where ρ is the density of vibrational levels. The vibrational period can be converted to the vibrational energy by noting that, in cm^{-1} , $\Delta E_{\text{vib}} = \nu/c = 1/(c\tau_v)$. We can use a similar transformation to define an energy associated with the collision, in cm^{-1} , as $\Delta E_{\text{col}} = 1/(c\tau_c)$. With these substitutions, eq 10 becomes

$$P_{\text{vib}} = \frac{\rho(E_i + \Delta E_{\text{vib}})}{\rho(E_i)} \exp[-|\Delta E_{\text{vib}}|/|E_{\text{col}}|] \quad (11)$$

This formula is essentially the same as eq 3 in ref 4, except that $d_{\text{force}}/v_{\text{loc}}$ has been replaced by $1/|E_{\text{col}}|$. We take E_{col} to be the value of the potential energy at the turning point. The absolute value for ΔE_{vib} is used as described previously;⁴ the probability falls off for either positive or negative ΔE_{vib} . The absolute value for E_{col} is included because the incoming velocity either pushes on the impact parameter (lever arm) when E_{col} is positive or pulls on it when E_{col} is negative; in either case it is the magnitude that matters. If not known, the density of states factors in the pre-exponential to eq 11 can be replaced by the classical values:

$$\frac{\rho(E_i + \Delta E_{\text{vib}})}{\rho(E_i)} = \left(\frac{E_i + \Delta E_{\text{vib}}}{E_i} \right)^{(s-1)+(1/2)} \quad (12)$$

where s is $3N - 6(5)$, and N is the number of atoms in the molecular target. We note that the current model extends the Landau–Teller theory to the case where there are many vibrational modes and where the density of vibrational levels is very high. A discussion of this extension is found in the section c under “Discussion of Assumptions” in that paper.⁴

In summary, the contribution to $P(J_f, \Delta E)$ from each turning point is given by $P_{\text{rot}}P_{\text{vib}}$, where J_f and ΔE are determined given by the solutions to eqs 6–8, where $\Delta E = \Delta E_{\text{rot}} + \Delta E_{\text{vib}}$, and where P_{rot} and P_{vib} are given by the above equations.

Computational Implementation of the Model. The inputs to the model are (a) the mass of the atomic collision partner, (b) the number of atoms in the target molecule, their masses, and their equilibrium positions, (c) an intermolecular potential describing the interaction of the incoming atom with the target molecule, (d) a table of bond stretches with Morse potential parameters (masses, bond dissociation energies, bond frequencies), and (e) the relative collision energy or translational temperature and the initial rotational level of the molecule or the rotational temperature. The intermolecular potential is often taken as a sum of pairwise interactions, but the model is not limited to this simple form. The table of bond stretching properties can be populated from standard tables of bond dissociation energies and frequencies. Additionally

needed are parameters describing the desired resolution of the joint probability distribution, for example, the minimum value of ΔE , the ΔE bin size, and number of ΔE bins, the minimum value of J_β , the J_f bin size and number of J_f bins. There is no computational penalty for choosing small bin sizes; only the storage increases.

The computation proceeds in two steps. First, a number of turning points are calculated, and second, the ΔE and J_f (or their ranges) are calculated for each turning point. A convenient feature of this approach is that the turning point calculation does not depend on J_i or rotational temperature, but only on the relative collision energy or the translational temperature. The second part of the calculation does depend on J_i or the rotational temperature, but the dependence on collision energy or translational temperature is contained in the results of the turning point calculation. This means that calculations for different J_i or rotational temperatures can use the same calculation of the turning points so long as the collision energy or translational temperature is the same.

Calculation of the turning points is performed using straight-line trajectories with an impact parameter chosen from a suitably weighted range and an orientation of the target molecule relative to the direction of the incoming atom chosen by random Euler angle rotations. When the energy at the turning point is positive, the criterion for the turning point is that the collision energy evaluated in a direction normal to the potential at the turning point should be equal to the potential of the rigid molecule at the turning point. When the energy at the turning point is negative, the criterion is that the turning point is the location where the incoming atom is closest to the point of zero potential energy. This latter selection is used to conform approximately with the trajectory criterion, which uses the distance of closest approach. Both of these turning point calculations require methods of successive approximations. Typically, 4000 turning points are sufficient to characterize the main features of the joint probability distribution, and these are formed in our implementation from 400 molecular orientations with 10 impact parameters for each orientation.

The calculation of ΔE and J_f (or their ranges) from each turning point proceeds as outlined in the section above. For each turning point, 1–5 values of the initial direction of J_i are chosen at random. In addition, five values of ΔE_{vib} are chosen by calculating the variation of potential energy at the turning point as the molecule vibrates. The vibration is modeled by the simple force field described above or is taken from frames of a trajectory, when available. Twelve random vibrational configurations are calculated or taken from the trajectory or force field, and five of these are chosen at random to determine ΔE_{vib} for any turning point. If only $V \leftrightarrow T$ transfer is allowed, then ΔE is changed by the amount of ΔE_{vib} , because $\Delta E = \Delta E_{\text{rot}} + \Delta E_{\text{vib}}$. If $V \leftrightarrow R$ transfer is allowed, then a random fraction of ΔE_{vib} is allowed to augment the collision energy so as to change the solution to the rotational energy transfer. This solution is obtained by treating the target molecule as a rigid body. The value of the final rotational level, J_β is determined by solving the coupled angular momentum and energy conservation equation for each component contributing to rotational change, the normal component and the component of the tangential motion that is perpendicular to the line of centers. Once a final state corresponding to J_f and $\Delta E = \Delta E_{\text{vib}} + \Delta E_{\text{rot}}$ is determined to satisfy the conservation laws, its probability is determined by the product of P_{rot} given in eq 9, and P_{vib} given in eq 11. These probabilities for each turning point are binned, summed, and

normalized to give the joint probability distribution. Typically, sufficient accuracy is obtained from the average of 400 orientations times 10 impact parameters each times 5 values of ΔE_{vib} each times 1–5 initial J_i orientations each, where the number of initial orientations increases with the magnitude of J_i . Computation of the turning points takes less than 1 CPU-hour, whereas computation of the JPD for a single J_i (or T_{rot}) and E_i (or T_{trans}) takes less than 30 CPU-min using *Mathematica* on a MacBook Air.

RESULTS: COMPARISON TO FULL TRAJECTORY CALCULATIONS

Evaluation of Assumptions Using Statistical Comparisons. Statistical analysis of results from each step of the computation helps to evaluate the model, as summarized in the following subsections.

Calculation of the Turning Points. The turning point calculation was investigated by detailed comparison to the trajectory results for argon collisions with *trans*-HOCO.³³ For both the model calculations and the trajectory calculations, we used the “Pairwise-18” potential. Comparison of the turning point distribution calculated by the model with the results of the trajectories is shown in Figure 3a, where the orientations and impact parameters are uncorrelated between the model and the trajectories. Figure 3b shows similar results but for model and trajectory calculations on allyl in its global minimum configuration (GM allyl).³² As is clear from these figures, the range and general shape of the distributions are in reasonable agreement.

Alternately, one can use the same orientation and impact parameter in the model as for each trajectory and compare the results. An informative method for comparison is to make correlation plots of model prediction and trajectory result for the same property; to the extent that the points fall on the (red) line of unit slope, the model and trajectory results agree. These plots can also be used to quantify the correlation by evaluating the R^2 parameter. For example, Figure 3c,d show the correlations for the total TP distance from the COM for the turning points with positive and negative potential energy, respectively, from data set of about 25 000 pairs. The R^2 values are 0.951 and 0.755, respectively. The agreement for the turning points with negative potential energy is not as good as for those with positive potential energy partly because the definition of turning point is not quite the same for the model and the trajectories.

It is clear from these results that the method for determining the turning points is reasonable and fairly accurate. It is interesting that it can be so successful given that the trajectory results are for a vibrating molecule and the model results are for a rigid one. Apparently, the turning points are determined largely by the equilibrium structure of the molecule, which is, of course, close to the vibrationally averaged structure.

Calculation of J_f and ΔE . The mapping between turning points and the variables of the joint probability distribution, J_f and ΔE , can also be compared between the model and the trajectories. A detailed comparison specific to each of the systems studied is presented in the sections that follow, whereas general correlations will be presented here. Several levels of the model were considered. The “standard” model, level 2, calculated the change in vibrational energy from the simple force field approach and assumed that all of the vibrational energy is exchanged to translation; i.e., no $V \leftrightarrow R$ energy transfer was considered. A simpler model, level 1, was also

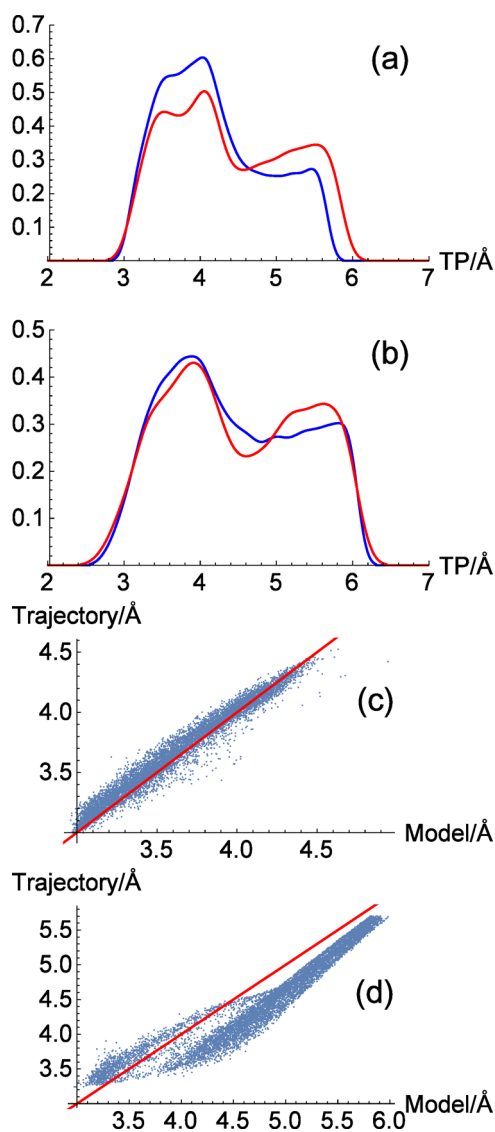


Figure 3. (a) Comparison of the turning point distributions for *trans*-HOCO between the model calculations (red) and the trajectory calculations (blue) for uncorrelated choices of impact parameters and orientations. (b) Similar data, except for model and trajectory calculations on allyl in its global minimum configuration. (c) Correlation plot for the total length of the vector from the COM to the TP for turning points with positive potential. (d) Correlation plot for the total length of the vector from the COM to the TP for turning points with negative potential.

considered in which no vibrational energy change is allowed—only rotational energy is exchanged. A more sophisticated model, level 3, was considered in which both $V \leftrightarrow T$ and $V \leftrightarrow R$ energy transfer were allowed. Finally, for systems where there were trajectory data that could be used to estimate the vibrational energy change at the turning point, these data were used in place of the simple force field approach.

We compared the model predictions to the results of several trajectory studies: argon with the allyl radical,^{3,32} argon with ethane,¹⁰ argon with pyrazine,¹⁰ argon with *trans*-HOCO,³³ argon with methane,³⁰ and helium with methane.²⁹ Considering all the combinations, we compared model predictions to trajectory results for four target molecules with a total of 14 conditions for which information on the complete JPD was available. In addition, there were 16 conditions for argon or

helium with methane for which some averaged information was available.^{29,30} An overview of the agreement between the model calculation and previous trajectory results can be made in the following way. For each trajectory result, we either calculate from the JPD or take from the reported results the values for the following moments of the distribution: $\langle \Delta E_{\text{up}} \rangle$, $\langle \Delta E_{\text{down}} \rangle$, $\langle \Delta E \rangle$, ΔE_{rms} , $\langle \Delta J_{\text{up}} \rangle$, $\langle \Delta J_{\text{down}} \rangle$, $\langle J_i \rangle$, and ΔJ_{rms} . Definitions of the first four of these are given in a paper by Jasper and Miller;²⁹ the last four are similarly defined. However, note that the sign convention for $\langle \Delta E_{\text{down}} \rangle$ is negative for our work and positive for that of Jasper and Miller. For the energy changes, there were a total of 89 comparison value pairs, whereas for the rotational changes there were a total of 44 comparison value pairs. For the level 2 model (including $V \leftrightarrow T$ transfer but not $V \leftrightarrow R$ transfer) and using trajectory data where available, the correlation plot of the predicted energy values vs the trajectory values shown in Figure 4a gives a nearly unit slope line with R^2

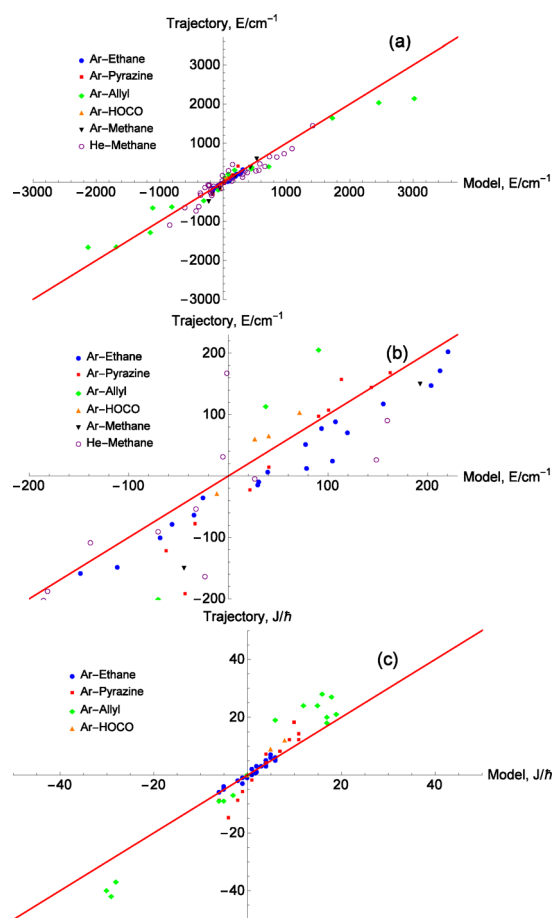


Figure 4. (a) Correlation plot for the model prediction of average energy changes of the trajectory results. (b) Expanded version of (a) emphasizing small energy changes. (c) Correlation plot for the model prediction of average rotational changes of the trajectory results. In all cases, the model calculation was level 2 and used trajectory results where available to determine the vibrational energy.

= 0.90. An expanded version of the plot near the origin of the axes is shown in Figure 4b. A similar plot in Figure 4c for the predicted rotational changes gives a quite accurate unit slope line with $R^2 = 0.86$. These and other combinations are listed in Table 2, from which several conclusions can be made. First, with the exception of those cases where $J_i = 0$, the level 1

Table 2. R^2 Values for Model Predictions of Trajectory Results

level	molecule set	vibration method	energy	rotational level
1	all except those with $J_i = 0$	(not relevant)	0.88	0.91
2	all	trajectory, where available	0.90	0.86
2	allyl, <i>trans</i> -HOCO	force field	0.83	0.88
2	allyl, <i>trans</i> -HOCO	trajectory	0.90	0.86
3	all	trajectory, where available	0.89	0.86

calculation is actually almost as good as level 2 or 3; that is, merely taking account of rotational energy transfer provides most of the solution. Of course, for cases where $J_i = 0$, it is not possible for ΔE to be smaller than zero if only rotational energy transfer is allowed, so for these cases, we must include some vibrational energy transfer. However, as seen from comparison on the second and last lines in the table, there is no better agreement by adding $V \leftrightarrow R$ transfer to $V \leftrightarrow T$ transfer. In addition, the calculation of the JPD is several times longer with inclusion of $V \leftrightarrow R$ transfer. Consequently, most of the detailed results to be presented below will be calculated with the Level 2 model. From lines three and four of the table, we see that use of the trajectory results rather than the simple force field model for the vibration improves slightly the agreement in rotational level moments of the distribution but has little effect on the energy moments.

More detailed comparisons for the individual systems follow.

Ar + Allyl with $J_i = 0, 136, 184,$ and 216 and $E_{\text{rel}} = 3500$ cm^{-1} . Trajectory results for the argon–allyl system have been reported previously.^{3,32} Figure 5 shows a comparison of the model predictions and the trajectory results for $J_i = 184$ using the level 2 version of the model and using trajectory results to determine the variation in TP energy with vibration. Similar results were obtained for $J_i = 0, J_i = 136,$ and $J_i = 216$. Table 3 summarizes the averaged results. In addition, for systems such as argon–allyl where the JPD, $P(J_f, \Delta E)$, from the trajectory results is reported, one can compare the probability in each model bin (of $J_f, \Delta E$) to the probability in each trajectory bin. For example, for the $J_i = 136, 184,$ and 216 systems, the JPD is binned into 80–92 ΔE bins times 15–25 J_f bins. For $J_i = 0$, there are 280 ΔE bins and 150 J_f bins. Most of these have low probabilities, contributing little to the sum of squared differences. Nevertheless, the R^2 values for the comparisons are useful. For $J_i = 0, R^2 = 0.19, J_i = 136, R^2 = 0.972,$ for $J_i = 184, R^2 = 0.95,$ and for $J_i = 216, R^2 = 0.49$.

Ar + Ethane with $J_i = 37.47, 18.74,$ and 9.38 for $T = 300$ K and with $J_i = 37.47, 26.50,$ and 18.74 for $T = 1200$ K. Trajectory results for the argon–ethane system have been reported previously.¹⁰ The JPD for the trajectory data has been summarized by a formula in the Supporting Information to ref 10 that is used here for comparison. For argon–ethane, argon–methane, and helium–methane the authors of the trajectory results employed Buckingham (or “Exponential-6”) intermolecular potentials. Though convenient and simple, this potential form has the disadvantage that as the distance approaches zero, the potential goes to negative infinity rather than to a positive number. The calculation of ΔE_{vib} requires that the potential at the turning point be evaluated as the molecule vibrates, and occasionally the vibration places an atom of the molecule in the region of the Buckingham potential that is unrealistic. For this

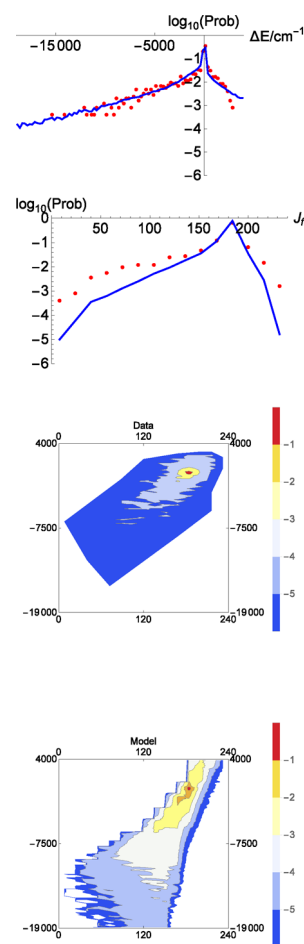


Figure 5. Joint probability distribution $P(J_f, \Delta E)$ for collisions of Ar with allyl starting in the GM configuration with $J_i = 184$ and for a collision energy of 10.0 kcal/mol (3500 cm^{-1}). The contours in the bottom two panels represent a log 10 scale of probability and are separated by 1.0 log units. The trajectory data contours are above those for the model results; the ordinate is $\Delta E/\text{cm}^{-1}$, and the abscissa is J_f/\hbar . The top panels give the trajectory results (red dots) and the model predictions (blue solid curve) for, on the top, the energy distribution summed over J_f and, below it, the rotational distribution summed over ΔE .

reason, our calculations were performed with a potential of a slightly different form given by Varandas and Rodrigues.⁴⁵ The Varandas–Rodrigues potential has 12 parameters. These were fit to give good agreement between the Varandas–Rodrigues and Buckingham potentials for Ar–C and Ar–H over the energy region up to 3000 cm^{-1} . The fits were excellent. For 800 comparison points in this energy region, the Varandas–Rodrigues Ar–H potential fit the Buckingham one with an $R^2 = 1.0$, whereas for the Ar–C potential the fit had an $R^2 = 0.9997$. The fitting parameters were for Ar–H, $\{C_6, C_8, C_{10}, R_0, A, b\} = \{31.6204, -2084.33, 12179.5, 2.84941, 18.5, 11.6957\}$, and for Ar–C, $\{C_6, C_8, C_{10}, R_0, A, b\} = \{219.915, 99.9992, 26512., 17.6855, 189.98, 1.95825\}$. In both cases, λ was taken as unity.

Figure 6 shows a comparison of the model predictions and the trajectory results for $J_i = 18.74$, with $T = 300$ K and for level 2 theory with the force field calculation of the vibrational change in energy at the TP. Similar plots were obtained for $J_i = 37.47$ and $J_i = 9.38$ with $T = 300$ K and for $J_i = 37.47, J_i = 26.50,$ and $J_i = 18.74$ with $T = 1200$ K. The trajectory results were

Table 3. Averaged Energy Transfer Parameters for Argon–Allyl Collisions^a

J_i	E_{trans}	$\langle \Delta E_{\text{up}} \rangle$	$\langle \Delta E_{\text{down}} \rangle$	$\langle \Delta E \rangle$	ΔE_{rms}
0	700	(91/205)	(-70/-201)	(38/113)	(190/310)
136	3500	(729/398)	(-1140/-1289)	(-297/-4714)	(1733/1641)
184	3500	(459/382)	(-1676/1658)	(-801/-632)	(2465/2034)
216	3500	(452/812)	(-2122/-2441)	(-1102/-677)	(3026/2139)
J_i	E_{trans}	$\langle \Delta J_{\text{up}} \rangle$	$\langle \Delta J_{\text{down}} \rangle$	$\langle \Delta J \rangle$	ΔJ_{rms}
0	700	(6/19)	(0/0)	(6/19)	(12/24)
136	3500	(19/21)	(-28/-37)	(-3/-7)	(15/24)
184	3500	(17/20)	(-29/-42)	(-5/-9)	(16/28)
216	3500	(17/18)	(-30/-40)	(-6/-9)	(18/27)

^aEnergies are in cm^{-1} and entries in parentheses give (model results/trajectory results^{3,32}).

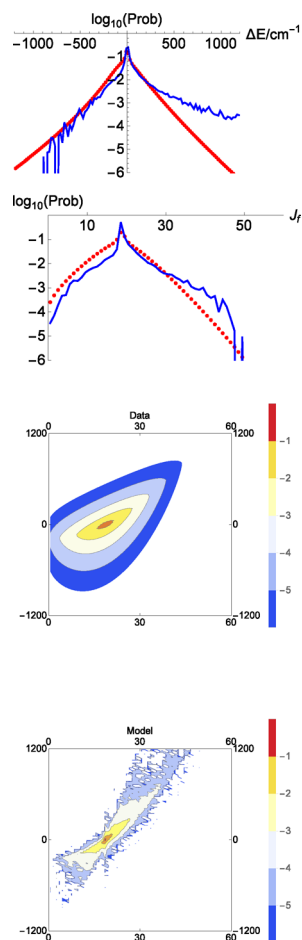


Figure 6. Joint probability distribution $P(J_f, \Delta E)$ for collisions of Ar with ethane with $J_i = 18.7$ and for a translational temperature of 300 K. The contours in the bottom two panels represent a log 10 scale of probability and are separated by 1.0 log units. The trajectory data contours are above those for the model results; the ordinate is $\Delta E/\text{cm}^{-1}$, and the abscissa is J_f/\hbar . The top panels give the trajectory results (red dots) and the model predictions (blue solid curve) for, on the top, the energy distribution summed over J_f and, below it, the rotational distribution summed over ΔE .

performed with a maximum impact parameter of 5–7, whereas the model calculations were performed with 6. Table 4 summarizes the averaged results. Comparison of the model and trajectory JPD values bin by bin gives the following results: for $T = 300$ K, $J_i = 9.38$, $R^2 = 0.17$, for $J_i = 18.74$, $R^2 = 0.54$, and for $J_i = 37.47$, $R^2 = 0.50$, and for $T = 1200$ K, $J_i = 18.74$, $R^2 = 0.71$, for $J_i = 26.50$, $R^2 = 0.63$, and for $J_i = 37.47$, $R^2 = 0.53$.

Ar + Pyrazine with $J_i = 82.6, 45.3$, and 22.6 , and $T = 300$ K. Trajectory results for the argon–pyrazine system have been reported previously.¹⁰ The JPD for the trajectory data has been summarized by a formula in the Supporting Information to ref 10 that is used here for comparison. Figure 7 shows a comparison of the model predictions and the trajectory results for $J_i = 45.3$ with $T = 300$ K. Similar plots were obtained for $J_i = 22.6$ and $J_i = 82.7$ with $T = 300$ K. The trajectory studies suggested a maximum impact parameter of 10, but this led to very few collisions that changed the energy. The radius of pyrazine at a potential energy of zero is less than 5, so we used a maximum impact parameter of 6. The net effect of this change is to decrease the prominence of the elastic peak. Table 5 summarizes the averaged results. Comparison of the model and trajectory JPD values bin by bin gives the following results. For $T = 300$ K we found for $J_i = 22.6$, $R^2 = 0.22$, for $J_i = 45.3$, $R^2 = 0.35$, and for $J_i = 82.7$, $R^2 = 0.30$.

Ar + *trans*-HOCO with $J_i = 0$ and $E_{\text{rel}} = 350$ cm^{-1} . Trajectory results for the argon–*trans*-HOCO system have been reported previously.³³ Figure 8 shows a comparison of the model predictions and the trajectory results for $J_i = 0$ using the level 2 model and the force field model for determination of the vibrational energy. The trajectory studies and the model calculations were both performed with 6.09 as the maximum impact parameter. Table 6 summarizes the averaged results. Comparison of the model and trajectory JPD values bin by bin gives $R^2 = 0.44$.

Ar + Methane with $T = 300$ – 2000 K. Trajectory results for the argon–methane system have been reported previously.³⁰ As mentioned above, for argon–ethane, argon–methane, and helium–methane, our calculations were performed with an equivalent Varandas–Rodrigues potential.⁴⁵ For 800 comparison points in this energy region, the Varandas–Rodrigues Ar–H potential fit the Buckingham one with an $R^2 = 1.0$, whereas for the Ar–C potential the fit also had an $R^2 = 1.0$. The fitting parameters were for Ar–H, $\{C_6, C_8, C_{10}, R_0, A, b\} = \{20.4295, 426.009, 12300, 7.2404, 8.44978, 1.65192\}$, and for Ar–C, $\{C_6, C_8, C_{10}, R_0, A, b\} = \{28.248, 1173.97, 26512., 15.6532, 199.653, 1.98589\}$. In both cases, λ was taken as unity.

Figure 9 shows the model predictions for $T = 1150$ K using level 2 and the force field method for estimating the vibrational energy. The detailed trajectory results were not published. Table 7 summarizes the averaged level-2 results for all of the conditions studied. The trajectory studies and the model calculations were both performed with 4.25 as the maximum impact parameter.

He + Methane with $J_i = 0$ – 40 and $T = 300$ – 2000 K. Trajectory results for the argon–methane system have been

Table 4. Averaged Energy Transfer Parameters for Argon–Ethane Collision^a

J_i	$T_{\text{trans}}, \text{K}$	$\langle \Delta E_{\text{up}} \rangle$	$\langle \Delta E_{\text{down}} \rangle$	$\langle \Delta E \rangle$	ΔE_{rms}
9.38	300	(77/51)	(-23/-36)	(39/6)	(119/70)
18.74	300	(94/77)	(-56/-79)	(31/-10)	(156/117)
37.47	300	(161/105)	(-215/-177)	(-34/-62)	(256/204)
18.74	1200	(204/147)	(-68/-101)	(105/24)	(274/206)
26.50	1200	(213/171)	(-111/-149)	(79/12)	(293/253)
37.47	1200	(221/202)	(-155/-212)	(30/-15)	(320/317)
J_i	$T_{\text{trans}}, \text{K}$	$\langle \Delta J_{\text{up}} \rangle$	$\langle \Delta J_{\text{down}} \rangle$	$\langle \Delta J \rangle$	ΔJ_{rms}
9.37	300	(2/3)	(-2/-2)	(2/1)	(4/4)
18.74	300	(4/3)	(-1/-3)	(1/0)	(4/4)
37.47	300	(1/2)	(-5/-4)	(-1/-1)	(4/5)
18.74	1200	(6/5)	(-1/-3)	(2/1)	(6/6)
26.50	1200	(3/3)	(-5/-5)	(1/0)	(5/6)
37.47	1200	(2/3)	(-6/-6)	(0/-1)	(5/7)

^a Energies are in cm^{-1} and entries in parentheses give (model results/trajectory results¹⁰).

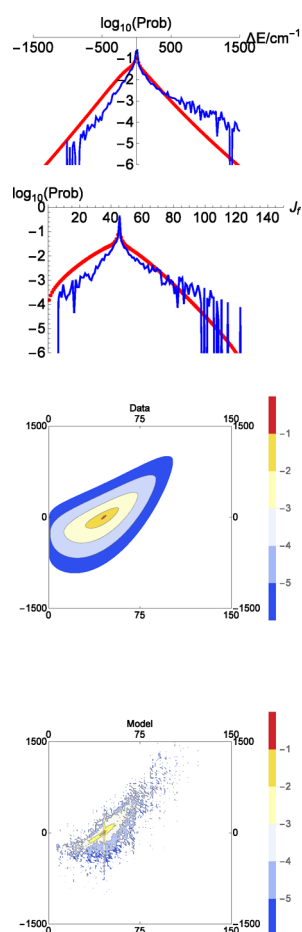


Figure 7. Joint probability distribution $P(J_f, \Delta E)$ for collisions of Ar with pyrazine with $J_i = 45.3$ and for a translational temperature of 300 K. The contours in the bottom two panels represent a log 10 scale of probability and are separated by 1.0 log units. The trajectory data contours are above those for the model results; the ordinate is $\Delta E/\text{cm}^{-1}$, and the abscissa is J_f/\hbar . The top panels give the trajectory results (red dots) and the model predictions (blue solid curve) for, on the top, the energy distribution summed over J_f and, below it, the rotational distribution summed over ΔE .

reported previously.²⁹ Our calculations again were performed with a potential of a slightly different form, as given by Varandas and Rodrigues.⁴⁵ The fits were excellent. For 730

comparison points in the relevant energy region, the Varandas–Rodrigues Ar–H potential fit the Buckingham one with an $R^2 = 0.9989$, whereas for the Ar–C potential the fit also had an $R^2 = 0.9989$. The fitting parameters were for Ar–H, $\{C6, C8, C10, R0, A, b\} = \{694.945, 1000.7, 12300, 10.9116, 14499.5, 2.5608\}$, and for Ar–C, $\{C6, C8, C10, R0, A, b\} = \{3800.12, 50.0013, 26512, 8.47305, 7600, 2.01001\}$. In both cases, λ was taken as unity.

Figure 10 shows the model predictions for $J_i = 20$ with $T = 1150$ K using level 2 and the force field method for estimating the vibrational energy. The detailed trajectory results were not published. Table 8 summarizes the averaged level-2 results for all of the conditions studied. The trajectory studies and the model calculations were both performed with 4.25 as the maximum impact parameter.

DISCUSSION

Insights from the Model. The most important finding of this study is that energy transfer in highly excited molecules is dominated by rotational energy transfer rather than by vibrational energy transfer. Even for a rigid molecule, by using conservation of angular momentum and energy, one can employ classical physics to determine the turning points and to predict from them the moments of the joint probability distribution with an $R^2 \approx 0.9$, provided that J_i is not too small. For small J_i , the solution to the rotational energy transfer needs to be augmented by a simple model to predict the change in energy at the turning point as the molecule vibrates. Some statistics from a few model results emphasize these points. Let $R_{\text{up}} \equiv \langle \Delta E_{\text{rot,up}} \rangle / \langle \Delta E_{\text{vib,up}} \rangle$ and $R_{\text{down}} \equiv \langle \Delta E_{\text{rot,down}} \rangle / \langle \Delta E_{\text{vib,down}} \rangle$. Table 9 shows some results. In all cases except for one, the R_{up} and R_{down} values are larger than unity, indicating that the amount of rotational energy transferred is larger than the amount of vibrational energy transferred, usually significantly so. The sole exception to this rule occurs in helium–methane where the target molecule is nearly spherical and colliding with a light atom, conditions such that rotational change due to motion normal to the potential is much less effective because the normal passes very close to the COM and because the small value of μ reduces the orbital angular momentum.

A second important finding is that there are two sources of rotational energy exchange, one due to motion normal to the potential energy surface and one due to motion tangential to the surface and perpendicular to the LOC. The first of these is

Table 5. Averaged Energy Transfer Parameters for Argon–Pyrazine Collisions^a

J_i	$T_{\text{trans}}, \text{K}$	$\langle \Delta E_{\text{up}} \rangle$	$\langle \Delta E_{\text{down}} \rangle$	$\langle \Delta E \rangle$	ΔE_{rms}
22.6	300	(91/96)	(-33/-79)	(42/13)	(144/143)
45.3	300	(101/106)	(-62/-123)	(22/-24)	(163/167)
82.7	300	(114/156)	(-154/-332)	(-43/-193)	(245/390)
J_i	$T_{\text{trans}}, \text{K}$	$\langle \Delta J_{\text{up}} \rangle$	$\langle \Delta J_{\text{down}} \rangle$	$\langle \Delta J \rangle$	ΔJ_{rms}
22.6	300	(11/12)	(-1/-6)	(4/4)	(11/14)
45.3	300	(4/7)	(-6/-9)	(1/-2)	(9/12)
82.7	300	(7/8)	(-4/-15)	(-2/9)	(10/18)

^aEnergies are in cm^{-1} and entries in parentheses give (model results/trajectory results¹⁰).

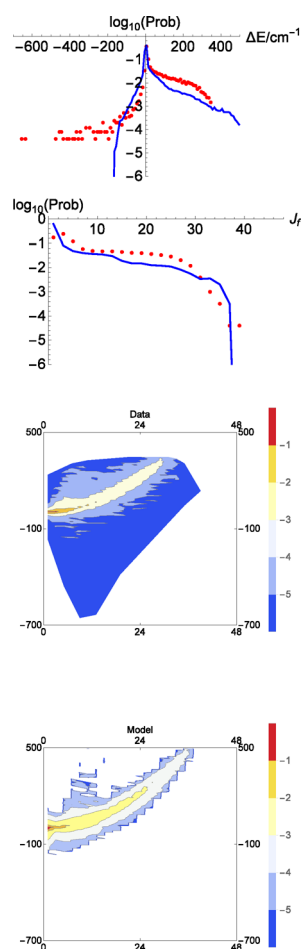


Figure 8. Joint probability distribution, $P(J_f, \Delta E)$, for collisions of Ar with *trans*-HOCO with $J_i = 0$ and $E_{\text{rel}} = 350 \text{ cm}^{-1}$. The contours in the bottom two panels represent a log 10 scale of probability and are separated by 1.0 log units. The trajectory data contours are above those for the model results; the ordinate is $\Delta E/\text{cm}^{-1}$, and the abscissa is J_f/\hbar . The top panels give the trajectory results (red dots) and the model predictions (blue solid curve) for, on the top, the energy distribution summed over J_f and, below it, the rotational distribution summed over ΔE .

expected from the work of McCaffery et al.^{46–48} who use a hard potential and calculate the rotational exchange from the motion normal to the hard surface. The second is less commonly realized and occurs only when there is a softer potential. Grazing collisions can cause rotational excitation from the tangential motion because the atom interacts with the tail of the potential, pushing or pulling on a long lever arm given by the distance from the COM to the TP along the LOC. The tangential excitation contributes mostly to small ΔJ . The

Table 6. Averaged Energy Transfer Parameters for Argon–*trans*-HOCO Collisions^a

J_i	$E_{\text{trans}}, \text{cm}^{-1}$	$\langle \Delta E_{\text{up}} \rangle$	$\langle \Delta E_{\text{down}} \rangle$	$\langle \Delta E \rangle$	ΔE_{rms}
0	350	(41/65)	(-11/-29)	(27/60)	(72/103)
J_i	$E_{\text{trans}}, \text{cm}^{-1}$	$\langle \Delta J_{\text{up}} \rangle$	$\langle \Delta J_{\text{down}} \rangle$	$\langle \Delta J \rangle$	ΔJ_{rms}
0	350	(5/9)	(0/0)	(5/9)	(8/12)

^aEnergies are in cm^{-1} and entries in parentheses give (model results/trajectory results³³).

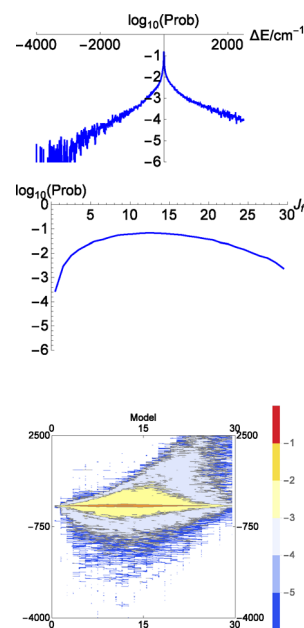


Figure 9. Model prediction for the joint probability distribution, $P(J_f, \Delta E)$, for collisions of Ar with methane for a translational and rotational temperature of 1150 K. The contours in the bottom two panels represent a log 10 scale of probability and are separated by 1.0 log units. The ordinate is $\Delta E/\text{cm}^{-1}$, and the abscissa is J_f/\hbar . The top panels give the model predictions for, on the top, the energy distribution summed over J_f and, below it, the rotational distribution summed over ΔE .

downward opening parabolas corresponding the rhs of eq 8 are relatively flat, partly because the impact parameter, equal to the distance to the TP, is large. Nonetheless, the tangential excitation can be an important component of the total. For example, for argon–allyl with $J_i = 0$ and $E_{\text{rel}} = 700 \text{ cm}^{-1}$, treating the tangential energy transfer as elastic rather than allowing it to induce rotational transfer reduces the value of $\langle \Delta E_{\text{up}} \rangle$ from 111 to 88 cm^{-1} and reduces the value of ΔE_{rms} from 216 to 186 cm^{-1} .

Table 7. Averaged Energy Transfer Parameters for Argon–Methane Collisions^a

T_{rot} , K	T_{trans} , K	$\langle \Delta E_{\text{up}} \rangle$	$\langle \Delta E_{\text{down}} \rangle$	$\langle \Delta E \rangle$	ΔE_{rms}
300	300	(108/ N/A)	(−44/−150)	(45/ N/A)	(193/150)
1150	1150	(269/ N/A)	(−159/−300)	(64/ N/A)	(440/390)
2000	2000	(327/ N/A)	(−218/−490)	(85/ N/A)	(539/600)
T_{rot} , K	T_{trans} , K	$\langle \Delta J_{\text{up}} \rangle$	$\langle \Delta J_{\text{down}} \rangle$	$\langle \Delta J \rangle$	ΔJ_{rms}
300	300	(8/N/A)	(0/N/A)	(8/N/A)	(9/N/A)
1150	1150	(15/N/A)	(0/N/A)	(15/N/A)	(16/N/A)
2000	2000	(18/N/A)	(0/N/A)	(18/N/A)	(19/N/A)

^aEnergies are in cm^{-1} and entries in parentheses give (model results/trajectory results²⁹).

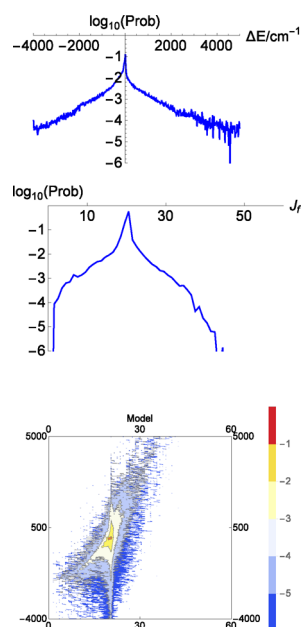


Figure 10. Model prediction for the joint probability distribution, $P(J_f, \Delta E)$, for collisions of He with methane for $J_i = 20$ and a translational temperature of 1150 K. The contours in the bottom two panel represent a log 10 scale of probability and are separated by 1.0 log units. The ordinate is $\Delta E/\text{cm}^{-1}$, and the abscissa is J_f/\hbar . The top panels give the model predictions for, on the top, the energy distribution summed over J_f and, below it, the rotational distribution summed over ΔE .

A third important finding is that rotational energy transfer is significant even for collisions where the potential at the TP is negative (attractive). For example, in argon colliding with *trans*-HOCO with $J_i = 0$ and $E_{\text{rel}} = 350 \text{ cm}^{-1}$, for 9376 positive potentials at the TP (out of 24 998), $\langle \Delta J \rangle = 16.3$ and $\langle \Delta E_{\text{rot}} \rangle = 129 \text{ cm}^{-1}$, whereas for 15 622 negative potentials at the TP, $\langle \Delta J \rangle = 4.4$ and $\langle \Delta E_{\text{rot}} \rangle = 18.2 \text{ cm}^{-1}$. Given that there are almost twice as many TPs with negative potentials as positive ones, the negative ones account for about half of the $\langle \Delta J \rangle$ and about one-quarter of the $\langle \Delta E_{\text{rot}} \rangle$.

A fourth important finding, corroborating our previous finding,⁴ is that energy transfer depends on the intermolecular potential very strongly, but only weakly on the intramolecular potential. The only features affected by the intramolecular potential are the calculation of how the energy at a TP varies with vibration and how the density of vibrational states varies with energy.

The model also allows one to interpret and predict the topology of the joint probability distribution. We start by considering the solution to the rotational energy transfer without vibration. Figure 11a shows the prediction of the joint probability distribution for $J_i = 20$ with $T_{\text{trans}} = 300 \text{ K}$ for helium colliding with methane. Because methane is a spherical rotor, there is a single rotational constant. The strong curved line is simply the map of rotational energy change as a function of J_f . The distribution of probability on this curve is determined by the solutions to eqs 7 and 8. A slightly different situation occurs when the target molecule is not a spherical rotor. For example, Figure 11b shows the rotation-only solution for argon–allyl with $J_i = 184$ and $E_{\text{rel}} = 3500 \text{ cm}^{-1}$. Because there is a range of rotational constants for different choices of the initial rotation direction with respect to the molecular framework, there is also a range of curvatures for the mapping of rotational energy as a function of J_f . All of the curves coincide at the elastic point where $\Delta E = 0$ and $J_f = J_i$, and the maximum probability is at this point. The distribution of probability elsewhere is determined again by the solutions to eqs 7 and 8. We now add $V \leftrightarrow T$ energy exchange to the picture, using the change of energy at each turning point to broaden ΔE . The result, shown in Figure 11c, is to broaden the result of Figure 11b in the vertical direction. The inclusion of $V \leftrightarrow R$ energy transfer further broadens slightly the joint probability distribution in the horizontal direction, as shown in Figure 11d.

One can now easily interpret some of the stranger joint probability distributions, such as, for example, that shown in the bottom contour of Figure 9. For this system, argon collides with methane with $T_{\text{trans}} = T_{\text{rot}} = 1150 \text{ K}$. Thus, J_i is chosen from a distribution corresponding to this temperature, and the joint probability distribution for rotation-only will be composed of several curves such as that in Figure 11a, each slightly displaced from the other and all having their maximum probability at the elastic point, where $\Delta E = 0$ and $J_f = J_i$. Inclusion of $V \leftrightarrow T$ transfer will broaden each of these curves along the ΔE axis, resulting in the contour shown in the bottom panel of Figure 9.

Highly Efficient Collisions. The model also provides insights into “highly efficient collisions” (HECs), sometimes called “supercollisions”. Highly efficient collisions have been observed and discussed in previous work^{20,21,23,49–52} and are defined as collisions with an energy transfer that is at least 5 times $\langle \Delta E_{\text{down}} \rangle$.⁵⁰ Both the model and the trajectory results show some probability for HECs. Our findings are that the HECs are a natural extension of the “normal” rotational and vibrational energy transfer that is responsible for less efficient collisions. No new mechanism is required to explain them. On the contrary, one can examine these collisions in detail and learn which parts of the normal distribution of input parameters is most responsible for them.

If we restrict ourselves to those systems and conditions for which there is trajectory data for the JPD that indicates a nonzero probability for HECs, then the average characteristics of these systems, taken from the model studies, can help provide insight as to the cause of this interesting energy transfer. Table 10 shows some of the characteristics. The columns labeled $P_{\text{model}}(\text{HEC})$ and $P_{\text{traj}}(\text{HEC})$ give the probabilities for HECs as calculated from the model and trajectory JPDs, respectively. The column $R_{\text{down}}(\text{HEC})$ gives $\langle \Delta E_{\text{rot,down}} \rangle / \langle \Delta E_{\text{vib,down}} \rangle$ considering only the HECs. The column R_{leverarm} gives the HEC/(all collision) ratio of average impact parameters for rotational excitation from motion normal

Table 8. Averaged Energy Transfer Parameters for Argon–Methane Collisions^a

J_i	$T_{\text{trans}}, \text{K}$	$\langle \Delta E_{\text{up}} \rangle$	$\langle \Delta E_{\text{down}} \rangle$	$\langle \Delta E \rangle$	ΔE_{rms}
0	300	(162/N/A)	(-228/-75)	(-5/31)	(316/126)
10	300	(134/N/A)	(-181/-188)	(-32/-54)	(317/198)
20	300	(154/N/A)	(-378/-282)	(-164/-109)	(553/285)
0	600	(161/N/A)	(-208/-77)	(-1/167)	(354/287)
10	600	(234/N/A)	(-185/-203)	(27/-5)	(391/245)
20	600	(279/N/A)	(-346/-337)	(-70/-91)	(573/303)
0	1150	(567/N/A)	(-252/-94)	(171/290)	(708/465)
10	1150	(410/N/A)	(-204/-294)	(131/90)	(664/399)
20	1150	(439/N/A)	(-375/-628)	(-23/-164)	(740/653)
30	1150	(433/N/A)	(-596/-654)	(-191/-264)	(972/726)
0	2000	(493/N/A)	(-277/-138)	(158/451)	(856/641)
20	2000	(763/N/A)	(-418/-740)	(149/26)	(1097/856)
40	2000	(749/N/A)	(-834/-1101)	(-171/-343)	(1423/1443)
J_i	$T_{\text{trans}}, \text{K}$	$\langle \Delta J_{\text{up}} \rangle$	$\langle \Delta J_{\text{down}} \rangle$	$\langle \Delta J \rangle$	ΔJ_{rms}
0	300	(1/N/A)	(0/N/A)	(1/N/A)	(2/N/A)
10	300	(1/N/A)	(-1/N/A)	(0/N/A)	(1/N/A)
20	300	(1/N/A)	(-1/N/A)	(0/N/A)	(2/N/A)
0	600	(1/N/A)	(0/N/A)	(1/N/A)	(3/N/A)
10	600	(1/N/A)	(-1/N/A)	(0/N/A)	(2/N/A)
20	600	(1/N/A)	(-2/N/A)	(0/N/A)	(2/N/A)
0	1150	(5/N/A)	(0/N/A)	(2/N/A)	(5/N/A)
10	1150	(1/N/A)	(-1/N/A)	(1/N/A)	(2/N/A)
20	1150	(1/N/A)	(-2/N/A)	(0/N/A)	(2/N/A)
30	1150	(1/N/A)	(-3/N/A)	(0/N/A)	(3/N/A)
0	2000	(3/N/A)	(0/N/A)	(3/N/A)	(5/N/A)
20	2000	(2/N/A)	(-2/N/A)	(1/N/A)	(3/N/A)
40	2000	(1/N/A)	(-2/N/A)	(0/N/A)	(3/N/A)

^aEnergies are in cm^{-1} and entries in parentheses give (model results/trajectory results²⁹).

Table 9. R_{up} and R_{down} for Selected Systems

system	J_i/T_{rot}	$E_{\text{trans}}/T_{\text{trans}}$	R_{up}	R_{down}
Ar–allyl	136	3500 cm^{-1}	3.1	1.9
Ar–ethane	37.5	1200 K	4.6	5.2
Ar–pyrazine	82.7	300 K	2.1	2.2
Ar– <i>trans</i> -HOCO	0	700 cm^{-1}	3.6	N/A
Ar–methane	2000 K	2000 K	3.3	2.8
He–methane	40	2000 K	0.8	0.9

to the potential. The final column gives the ratio of the average potential at the turning point for the HECs to that for all collisions. First, we note that HECs seem to be a natural occurrence in many of the systems studied, especially in cases when J_i is relatively high so that substantial rotational energy may be lost. Second, they are associated with larger than average lever arms (impact parameters) for excitation along the normal to the potential and with larger than average potentials at the TP. The two observations taken together mean both that the velocity normal to the potential is larger than average and the impact parameter is larger, giving larger rotational excitation. In addition, because the amount of vibrational energy available to the collision depends on how strongly the potential changes with vibration, this amount will normally be larger when the potential is higher. Furthermore, the probability for such vibrational energy transfer, given in eq 11 is relatively large because the collision energy is high. Consequently, both ΔE_{rot} and ΔE_{vib} are large for such conditions. Still, in most cases, the rotational excitation is stronger, as can be seen by the observation that R_{down} (HECs) is generally larger than unity. In terms of the solid curves in

Figure 2a, the high values of the potential and the impact parameter mean that the solid blue parabola has strong curvature, such that it intersects the solid red rotational energy curve very near $J_f = 0$. The picture that this provides for HECs is that they are due to “sweet spots” in the orientation/impact parameter space where the distance between the COM and the surface normal through the TP is large and where the potential at the turning point is high.

Limitations of the Model and Suggestions for Future Studies. As successful as the model appears to be, it should be noted that it is limited. First, it is almost entirely based on classical mechanics. The rotational problem is treated classically; rotational energies are taken as $J^2 B$ with J allowed to be nonintegral. The available vibrational energy is also treated classically, although the probability of transfer is treated by the adiabaticity principle, a concept that can be derived from quantum first-order perturbation theory. If quantum effects are expected to be important, this theory will begin to fail. However, it seems likely that for systems such as those described above, where there are many energy states populated and where the excitation energy is several electronvolts, quantum effects can likely be neglected in most cases.

There are two principal weak aspects of the model. The first is that it is difficult and somewhat arbitrary to determine TPs for trajectories along impact parameters that do not sample the repulsive part of the potential. The method chosen sets the TP as the point at which the distance between the straight-line trajectory and the zero of potential energy is shortest. A better method that might be explored is actually to integrate the trajectory of the incoming atom using just the intermolecular potential and then to choose the distance of closest approach.

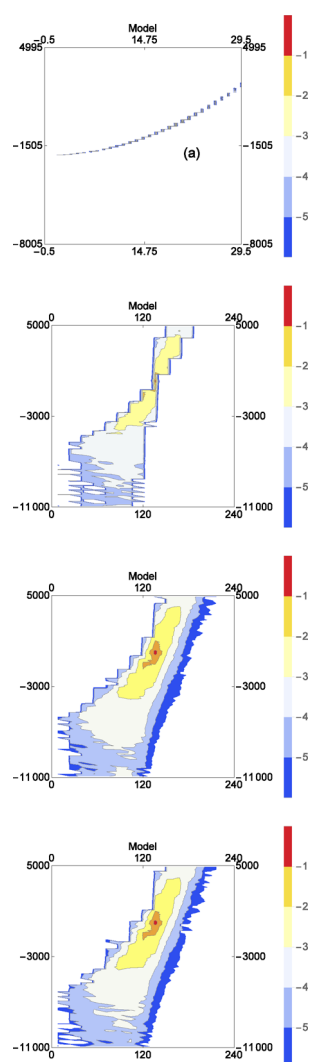


Figure 11. Topology of the joint probability distribution (JPD), $P(J_\beta \Delta E)$. The contours represent a log 10 scale of probability and are separated by 1.0 log units. The ordinate is $\Delta E/\text{cm}^{-1}$, and the abscissa is J_β/\hbar . Panel a is the JPD for helium–methane collisions with $J_i = 20$ and $T_{\text{trans}} = 300$ K considering only rotational energy transfer. The next three panels are for argon–allyl collisions with $J_i = 136$ and $E_{\text{rel}} = 3500$ cm^{-1} and with rotation only (b), with rotation and $V \leftrightarrow T$ energy transfer (c), and with rotation and $V \leftrightarrow R, T$ energy transfer (d).

This approach should give the maximum agreement with the trajectories. However, this approach would increase the time of the calculation and might not be successful, because it would still not take into account any rearrangement of the molecule as the atom gets close.

The second aspect of the model that could be improved is the force field used to calculate the change in vibrational energy at the turning point. The current model uses only stretching motions in the target molecule. Use of data from the trajectories on how the molecule vibrates improves the agreement between the model predictions and the trajectory calculations, so it appears that the model would benefit from a more complete force field. On the contrary, because most of the accuracy of the model is achieved by a calculation considering rotation alone, it seems unlikely that even an exact force field would significantly improve the calculation, except perhaps for downward energy transfers when $J_i = 0$.

An extension of the model might be made to consider energy transfer between a target molecule and another molecule, as opposed to an atom such as helium or argon. We are currently investigating energy transfer from highly excited methane colliding with water, and it is possible that the model can provide some insight, if not accurate calculation, of the energy transfer properties for this system.

SUMMARY AND CONCLUSIONS

A model for energy transfer in the collision of a highly excited target molecule with an atom has been developed and tested by comparing its predictions with the results of trajectory calculations. The model predicts selected moments of the joint probability distribution, $P(J_\beta \Delta E)$, with an $R^2 \approx 0.90$. Energy transfer is dominated by rotational change, and vibrational change is smaller by comparison. The rotational change can be predicted from classical mechanics and solution to the conservation laws of angular momentum and energy. There are two main mechanisms for rotational energy transfer, one involving motion normal to the potential energy contours and one involving motion tangential to the potential energy contours and perpendicular to the line of centers. The model allows insights concerning both the general topology of the joint probability distribution and the presence of highly efficient collisions. The latter are seen to be normal consequences of the energy transfer model. They are due mostly to rotational energy transfer and involve collision at “sweet spots” in the space of impact parameter and molecular orientation.

Table 10. Characteristics of Highly Efficient Collisions

system	J_i	$E_{\text{trans}}/T_{\text{trans}}$	$P_{\text{model}}(\text{HEC})$	$P_{\text{tra}}(\text{HEC})$	$R_{\text{down}}(\text{HECs})$	$R_{\text{lever arm}}$	$\frac{\langle V_{\text{TP}}(\text{HEC}) \rangle}{\langle V_{\text{TP}} \rangle}$
Ar–allyl	136	3500 cm^{-1}	0.018	0.012	1.26	1.27	4.16
Ar–allyl	184	3500 cm^{-1}	0.023	0.011	5.81	1.32	2.61
Ar–allyl	216	3500 cm^{-1}	0.006	0.003	16.1	1.36	2.35
Ar–ethane	37.47	300 K	0.014	0.003	65.3	1.73	2.13
Ar–ethane	18.74	300 K	0.013	0.006	9.60	1.55	3.35
Ar–ethane	9.37	300 K	0.006	0.011	0.09	1.23	10.21
Ar–ethane	37.47	1200 K	0.021	0.004	11.2	1.30	1.98
Ar–ethane	26.50	1200 K	0.013	0.009	6.18	1.325	2.20
Ar–ethane	18.74	1200 K	0.011	0.013	0.71	1.21	4.82
Ar–pyrazine	45.27	300 K	0.009	0.003	0.44	1.71	−14.3 ^a
Ar–pyrazine	22.64	300 K	0.014	0.011	−0.06	1.70	−13.4 ^a

^aThe average potential for all collisions is negative for these conditions.

■ AUTHOR INFORMATION

Corresponding Authors

*P. L. Houston. E-mail: paul.houston@cos.gatech.edu.

*R. Conte. E-mail: riccardo.conte@emory.edu.

*J. M. Bowman. Email: jmbowma@emory.edu.

Notes

The authors declare no competing financial interest.

■ ACKNOWLEDGMENTS

This material is based upon work supported by the U.S. Department of Energy, Office of Science, Office of Basic Energy Sciences, under Award Number DE-FG02-97ER14782. We appreciate conversations with Ahren Jasper and John Barker.

■ REFERENCES

- (1) Lindemann, F. A. Discussion on the Radiation Theory of Chemical Action. *Trans. Faraday Soc.* **1922**, *17*, 598–599.
- (2) Christiansen, J. A.; Kramers, H. A. Velocity of Chemical Reactions. *Z. Phys. Chem.* **1923**, *104*, 451–471.
- (3) Conte, R.; Houston, P. L.; Bowman, J. M. Trajectory Study of Energy Transfer and Unimolecular Dissociation of Highly Excited Allyl with Argon. *J. Phys. Chem. A* **2014**, *118*, 7742–7757.
- (4) Houston, P. L.; Conte, R.; Bowman, J. M. Collisional Energy Transfer in Highly Excited Molecules. *J. Phys. Chem. A* **2014**, *118*, 7742–7757.
- (5) Troe, J. Theory of Thermal Unimolecular Reactions at Low Pressures. I. Solutions of the Master Equation. *J. Chem. Phys.* **1977**, *66*, 4745–4757.
- (6) Troe, J. Theory of Thermal Unimolecular Reactions at Low Pressures. II. Strong collision rate constants. Applications. *J. Chem. Phys.* **1977**, *66*, 4758–4775L.
- (7) Gilbert, R. G. Theory of Collisional Energy Transfer of Highly Excited Molecules. *Int. Rev. Phys. Chem.* **1991**, *10*, 319–347.
- (8) Barker, J. R.; Yoder, L. M.; King, K. D. Vibrational Energy Transfer Modeling of Nonequilibrium Polyatomic Reaction Systems. *J. Phys. Chem. A* **2001**, *105*, 796–809.
- (9) Barker, J. R.; Golden, D. M. Master Equation Analysis of Pressure-Dependent Atmospheric Reactions. *Chem. Rev.* **2003**, *103*, 4577–4591.
- (10) Barker, J. R.; Weston, R. E., Jr. Collisional Energy Transfer Probability Densities $P(E, J; E', J')$ for Monatomics Colliding with Large Molecules. *J. Phys. Chem. A* **2010**, *114*, 10619–10633.
- (11) Barker, J. R.; Weston, R. E. Correction to “Collisional Energy Transfer Probability Densities $P(E, J; E', J')$ for Monatomics Colliding with Large Molecules”. *J. Phys. Chem. A* **2012**, *116*, 799–799.
- (12) Tardy, D. C. Competitive Stabilization - New Method for Obtaining Vibrational Energy-Transfer Probabilities in Chemical Activation Systems. *ACS Abstr.* **1977**, *173* ((MAR20)), 175–175.
- (13) Smith, G. P.; Barker, J. R. Energy-Transfer Rates for Vibrationally Excited Gas-phase Azulene in the Electronic Ground State. *Chem. Phys. Lett.* **1981**, *78*, 253–258.
- (14) Barker, J. R. Direct Measurements of Energy-Transfer Involving Large Molecules in the Electronic Ground-State. *J. Phys. Chem.* **1984**, *88*, 11–18.
- (15) Barker, J. R.; Toselli, B. M. Infrared-Emission Studies of the Vibrational Deactivation of Benzene Derivatives. *Int. Rev. Phys. Chem.* **1993**, *12*, 305–338.
- (16) Hippler, H.; Troe, J.; Wendelken, H. J. Direct Observation of Collisional Deactivation of Highly Excited Toluene. *Chem. Phys. Lett.* **1981**, *84*, 257–259.
- (17) Hippler, H.; Lindemann, L.; Troe, J. Collisional Energy Transfer of Vibrationally Highly Excited Molecules. V. UV Absorption Study of Azulene. *J. Chem. Phys.* **1985**, *83*, 3906–3912.
- (18) Hippler, H.; Troe, J. Recent Direct Studies of Collisional Energy Transfer on Vibrationally Excited Molecules in the Electronic Ground State In *Advances in Gas-Phase Photochemistry and Kinetics: Bimolecular*

Collisions; Ashfold, M. N. R., Baggott, J. E., Eds.; The Royal Society of Chemistry: London, 1989; p 209.

(19) Hold, U.; Lenzer, T.; Luther, K.; Reihs, K.; Symonds, A. Collisional Energy Transfer Probabilities in the Deactivation of Highly Vibrationally Excited Aromatics. *Ber. Bunsen-Ges. Phys. Chem.* **1997**, *101*, 552–565.

(20) Wall, M. C.; Mullin, A. S. Supercollision” Energy Dependence: State-resolved Energy Transfer in Collisions Between Highly Vibrationally Excited Pyrazine (Evib = 37,900 cm⁻¹ and 40,900 cm⁻¹) and CO₂. *J. Chem. Phys.* **1998**, *108*, 9658–9667.

(21) Wall, M. C.; Lemoff, A. S.; Mullin, A. S. Independent Determination of Supercollision Energy Loss Magnitudes and Rates in Highly Vibrationally Excited Pyrazine with Evib = 36,000–41,000 cm⁻¹. *J. Phys. Chem. A* **1998**, *102*, 9101–9105.

(22) Pashutzki, A.; Oref, I. Collision-induced Dissociation of Cyclohexadiene by a Vibrationally Hot Collider. *J. Phys. Chem.* **1988**, *92*, 178–182.

(23) Liu, C.-L.; Hsu, H. C.; Lyu, J.-J.; Ni, C.-K. Supercollisions and Energy Transfer of Highly Vibrationally Excited Molecules. *J. Chem. Phys.* **2005**, *123*, 131102.

(24) Brown, N. J.; Miller, J. A. Collisional Energy Transfer in the Low-pressure Limit: Unimolecular Dissociation of HO₂. *J. Chem. Phys.* **1984**, *80*, 5568–5580.

(25) Whyte, A. R.; Gilbert, R. G. A Classical Trajectory Calculation of Average Energy Transfer Parameters for the CH₃OO + Ar System. *Aust. J. Chem.* **1989**, *442*, 1227–1234.

(26) Lim, K. F.; Gilbert, R. G. Calculation of Collisional-Energy-Transfer Rates in Highly Excited Molecules. *J. Phys. Chem.* **1990**, *94*, 72–77.

(27) Lendvay, G.; Schatz, G. C. Comparison of Master Equation and Trajectory Simulation of the Relaxation of an Ensemble of Highly Vibrationally Excited Molecules. *J. Phys. Chem.* **1994**, *98*, 6530–6536.

(28) Lenzer, T.; Luther, K.; Troe, J.; Gilbert, R. G.; Lim, K. F. Trajectory Simulations of Collisional Energy Transfer in Highly Excited Benzene and Hexafluorobenzene. *J. Chem. Phys.* **1995**, *103*, 626–641.

(29) Jasper, A. W.; Miller, J. A. Collisional Energy Transfer in Unimolecular Reactions: Direct Classical Trajectories for CH₄ + H in Helium. *J. Phys. Chem. A* **2009**, *113*, 5612–5619.

(30) Jasper, A. W.; Miller, J. A. Theoretical Unimolecular Kinetics for CH₄ + M ⇌ CH₃ + H + M in Eight Baths, M = He, Ne, Ar, Kr, H₂, N₂, CO, CH₄. *J. Phys. Chem. A* **2011**, *115*, 6438–6455.

(31) Jasper, A. W.; Miller, J. A.; Klippenstein, S. J. The Collision Efficiency of Water in the Unimolecular Reaction CH₄ (+H₂O) → CH₃ + H (+H₂O): One-Dimensional and Two-Dimensional Solutions of the Low-Pressure-Limit Master Equation. *J. Phys. Chem. A* **2013**, *117*, 12243–12255.

(32) Conte, R.; Houston, P. L.; Bowman, J. M. Classical Trajectory Study of Energy Transfer in Collisions of Highly Excited Allyl Radical with Argon. *J. Phys. Chem. A* **2013**, *117*, 14028–14041.

(33) Conte, R.; Houston, P. L.; Bowman, J. M. Communication: A Benchmark-Quality, Full-dimensional ab initio Potential Energy Surface for Ar-HOCO. *J. Chem. Phys.* **2014**, *140*, 151101.

(34) Barker, J. R. A State-to-State Statistical-dynamical Theory for Large Molecule Collisional Energy Transfer. *Ber. Bunsen-Ges. Phys. Chem.* **1997**, *101*, 566–573.

(35) Nordholm, S.; Freasier, B. C.; Jolly, D. L. Ergodic Collision Theory of Intermolecular Energy Transfer. *Chem. Phys. Lett.* **1977**, *25*, 433–449.

(36) Freasier, B. C.; Jolly, D. L.; Nordholm, S. Ergodic Collision Theory of Intermolecular Energy Transfer II. Quantum Effects in the Harmonic Approximation. *Chem. Phys.* **1978**, *32*, 161–168.

(37) Ming, L.; Sewell, T. D.; Nordholm, S. A Simulation Study of Energy Transfer in Methyl Isocyanide-Inert Gas Collisions. *Chem. Phys.* **1995**, *199*, 83–104.

(38) Ming, L.; Davidsson, J.; Nordholm, S. Energy Transfer in Collisions of Small Gas-Phase Clusters - Comparison of Molecular Dynamics and Statistical limit Estimates. *Chem. Phys.* **1995**, *201*, 121–140.

- (39) Ming, L.; Davidsson, J.; Nordholm, S. Molecular Dynamics Study of Energy Transfer in Binary Collisions of Water Molecules. *J. Chem. Phys.* **1996**, *104*, 9001–9015.
- (40) Nilsson, D.; Nordholm, S. Statistical Model of Energy Transfer in Molecular Collisions: De-energization of Highly Excited Toluene. *J. Chem. Phys.* **2002**, *116*, 7040–7048.
- (41) Nilsson, D.; Nordholm, S. Modeling Energy Transfer in Molecular Collisions: Statistical Theory versus Experiment for Highly Excited Toluene and Azulene. *J. Chem. Phys.* **2003**, *119*, 11212–11220.
- (42) Nilsson, D.; Nordholm, S. Statistical Theory of Collisional Energy Transfer in Molecular Collisions. Trans-Stilbene Deactivation by Argon, Carbon Dioxide, and n-Heptane. *J. Phys. Chem. A* **2006**, *110*, 3289–3296.
- (43) Lenzer, T.; Luther, K.; Nilsson, D.; Nordholm, S. PECT Model Analysis and Predictions of Experimental Collisional Energy Transfer Probabilities $P(E',E)$ and Moments (ΔE) for Azulene and Biphenylene. *J. Phys. Chem. B* **2005**, *109*, 8325–8331.
- (44) Jasper, A. W.; Plezler, K. M.; Miller, J. A.; Karmarchik, E.; Harding, L. B.; Klippenstein, S. J. Predictive a priori Pressure-dependent Kinetics. *Science* **2014**, *346*, 1212–1215.
- (45) Varandas, A. J. C.; Rodrigues, S. P. J. Double Many-Body Expansion Potential Energy Surface for Ground-State HCN Based on Realistic Long Range Forces and Accurate ab initio Calculations. *J. Chem. Phys.* **1997**1069647–9658.
- (46) McCaffery, A. J.; Proctor, M. J.; Whitaker, B. J. Rotational Energy Transfer: Polarization and Scaling. *Annu. Rev. Phys. Chem.* **1986**, *37*, 223–244.
- (47) McCaffery, A. J.; Alwahabi, Z. T.; Osborne, M. A.; Williams, C. J. Rotational Transfer, an Angular Momentum Model. *J. Chem. Phys.* **1993**, *98*, 4586–4602.
- (48) McCaffery, A. J.; New, A. Approach to Molecular Collision Dynamics. *Phys. Chem. Chem. Phys.* **2004**, *6*, 1637–1657.
- (49) Bernshtein, V.; Oref, I. Effect of Supercollisions on Chemical Reactions in the Gas Phase. *J. Phys. Chem.* **1993**, *97*, 12811–12818.
- (50) Clary, D. C.; Gilbert, R. G.; Bernshtein, V.; Oref, I. Mechanisms for Supercollisions. *Faraday Discuss. Chem. Soc.* **1995**, *102*, 423–433.
- (51) Li, Z.; Sansom, R.; Bonella, S.; Coker, D. F.; Mullin, A. S. Trajectory Study of Supercollision Relaxation in Highly Vibrationally Excited Pyrazine and CO₂. *J. Phys. Chem. A* **2005**, *109*, 7657–7666.
- (52) Liu, C.-L.; Hsu, H. C.; Hsu, Y. C. Energy Transfer of Highly Vibrationally Excited Naphtalene. I. Translational Collision Energy Dependence. *J. Chem. Phys.* **2007**, *127*, 104311.